Charge transport and photocurrent generation in poly (3-hexylthiophene)

Mihailetchi, VD; Xie, HX; de Boer, B; Koster, LJA; Blom, PWM; Mihailetchi, Valentin D.; Xie, Hangxing

Published in:
Advanced Functional Materials

DOI:
10.1002/adfm.200500420

Publication date:
2006

DOI: 10.1002/adfm.200500420

Charge Transport and Photocurrent Generation in Poly(3-hexylthiophene):Methanofullerene Bulk-Heterojunction Solar Cells**

By *Valentin D. Mihailetchi*, *Hangxing Xie*, *Bert de Boer*, *L. Jan Anton Koster*, and *Paul W. M. Blom**

The effect of controlled thermal annealing on charge transport and photogeneration in bulk-heterojunction solar cells made from blend films of regioregular poly(3-hexylthiophene) (P3HT) and methanofullerene (PCBM) has been studied. With respect to the charge transport, it is demonstrated that the electron mobility dominates the transport of the cell, varying from 10^{-8} $m^2 V^{-1} s^{-1}$ in as-cast devices to $\approx 3 \times 10^{-7}$ $m^2 V^{-1} s^{-1}$ after thermal annealing. The hole mobility in the P3HT phase of the blend is dramatically affected by thermal annealing. It increases by more than three orders of magnitude, to reach a value of up to $\approx 2 \times 10^{-8}$ $m^2 V^{-1} s^{-1}$ after the annealing process, as a result of an improved crystallinity of the film. Moreover, upon annealing the absorption spectrum of P3HT:PCBM blends undergo a strong red-shift, improving the spectral overlap with solar emission, which results in an increase of more than 60 % in the rate of charge-carrier generation. Subsequently, the experimental electron and hole mobilities are used to study the photocurrent generation in P3HT:PCBM devices as a function of annealing temperature. The results indicate that the most important factor leading to a strong enhancement of the efficiency, compared with non-annealed devices, is the increase of the hole mobility in the P3HT phase of the blend. Furthermore, numerical simulations indicate that under short-circuit conditions the dissociation efficiency of bound electron–hole pairs at the donor/acceptor interface is close to 90 %, which explains the large quantum efficiencies measured in P3HT:PCBM blends.

1. Introduction

Organic photovoltaic devices prepared from composite films of functionalized fullerenes as electron acceptors (A) and conjugated polymers as electron donors (D) have recently evolved as promising cost-effective alternatives to conventional inorganic solar cells.[1–3] Unlike inorganic solar cells, photon absorption in bulk-heterojunction (BHJ) D/A organic cells mainly creates excited electron–hole pairs (excitons) that subsequently dissociate at a heterojunction interface via an ultrafast charge transfer (≈45 fs) from the exited donor to the acceptor.[4] After dissociation, a geminate pair of a hole at the donor and an electron at the acceptor is formed across the interface, which further needs to be separated into free charge carriers through the assistance of an electric field. These photogenerated free holes and electrons are then transported through the donor and acceptor phases towards the electrodes, resulting in an external photocurrent density (J_{ph}). As a result, the external photocurrent does not solely depend on the photogeneration rate of free electrons and holes, but also on the transport properties of the electrons and holes in the acceptor and donor, respectively. Most of the previous work on the physics of BHJ solar cells was performed on blends of poly(2-methoxy-5-(3′,7′-dimethyloctyloxy)-*p*-phenylene vinylene) (MDMO-PPV) and soluble fullerene derivatives such as [6,6]-phenyl C_{61}-butyric acid methyl ester (PCBM). The power conversion efficiencies (ηs) reported for this type of devices, measured under AM 1.5 (air mass 1.5) standard test conditions,[5] range from 2.5 to 3 %.[6,7] However, to achieve these efficiencies, up to 80 wt.-% of PCBM, a material which barely contributes to the absorption, has to be added into the MDMO-PPV:PCBM mixture. Recently, we demonstrated that one of the main reasons for this relatively large amount of PCBM being required is the enhancement of the hole transport in MDMO-PPV, which is the slowest carrier, when blended with PCBM.[8] Furthermore, a too-low hole mobility will also lead to a buildup of space-charge in the solar cell, which is detrimental to the fill factor and efficiency.[9] Therefore, an intrinsically higher hole mobility in the blend permits one to reduce the amount of PCBM and inhibits the occurrence of space-charge, which will further increase the magnitude of the photogenerated current and enhance the η.

Among the materials investigated so far, regioregular poly(3-hexylthiophene) (P3HT) has demonstrated promising

[*] Prof. P. W. M. Blom, V. D. Mihailetchi, H. X. Xie, Dr. B. de Boer, L. J. A. Koster
Materials Science Centre, University of Groningen
Nijenborgh 4, NL-9747 AG Groningen (The Netherlands)
E-mail: P.W.M.Blom@rug.nl
L. J. A. Koster
Dutch Polymer Institute, University of Groningen
Nijenborgh 4, NL-9747 AG Groningen (The Netherlands)

[**] The authors are indebted to J. C. Hummelen for fruitful discussions and the generous supply of PCBM, and Minte Mulder for technical assistance. The work of L. J. A. Koster forms part of the research program of the Dutch Polymer Institute (#323).

physical properties, such as environmental stability, reasonably high hole mobility, and an improved absorption as compared with PPV-based devices. Thermal annealing of the P3HT:PCBM-blend devices dramatically improves the external quantum efficiency and η of these cells.[10–12] It is well known that an enhanced degree of crystallinity can be induced in polythiophene films by thermal annealing. This controlled crystallization and orientation of polythiophene polymer chains can significantly improve the hole mobility. After annealing, energy conversion efficiencies as high as 3.5 % have been reported.[12,13] Besides this, a red-shift of the optical absorption of P3HT inside the blend is observed, providing an improved overlap with the solar emission.

Figure 1 shows the experimental J_{ph} of such P3HT:PCBM blends (50:50 wt.-%) in a double-logarithmic plot as a function of effective applied voltage (V_0–V).[14] The curves correspond to different postproduction treatments: as-cast, thermally annealed at a temperature where the enhancement in η is maximized (120 °C), and annealed at a lower temperature (70 °C). Thermal annealing was performed on complete devices, i.e., with the photoactive layer between the electrodes, on the hot plate for a period of four minutes. It appears from Figure 1 that the photocurrent shows a strong enhancement after thermal annealing. For the completely annealed device (annealed at 120 °C), the short-circuit current (J_{SC}) increases by a factor of five, the fill factor (FF) increases by a factor of two, and the overall enhancement of η is about one order of magnitude, when compared with the device as cast. This dramatic boost in the efficiency as a result of thermal treatment of the photoactive layer has been suggested to be caused by the burning of shunts,[12] an increase in hole mobility owing to crystallization of the polymer, a better morphology, or an improved overlap with the solar emission resulting from the red-shift of the optical absorption.[10–12,15] However, the effect of the thermal-annealing process on the solar-cell performance in terms of physical parameters, such as the charge-carrier mobility and photocurrent generation efficiency, in these devices has not been quantified.

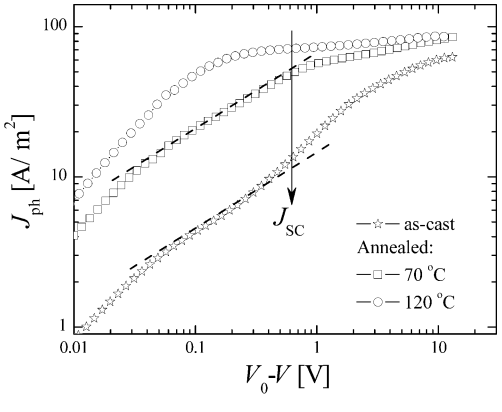

Figure 1. Experimental photocurrent (J_{ph}) versus effective applied voltage ($V_0 - V$) of the P3HT:PCBM devices at room temperature for as-cast devices and after thermally annealing of the photoactive layers (see legend). The thickness of the devices (L) is 96 nm and the arrow indicates the position of the short-circuit current (J_{SC}). The dashed lines represent the square-root dependence of the J_{ph} on voltage.

Recently, we have developed a device model which quantitatively describes the behavior of PPV:PCBM BHJ solar cells. We have shown that the dissociation efficiency of bound electron–hole (e–h) pairs, created after photoinduced electron transfer at the D/A interface, is an important limiting factor in photovoltaic devices based on this materials system.[8,16,17] Furthermore, with regard to the charge transport, we demonstrated that the photocurrent reaches the fundamental space-charge limit when the difference in electron and hole mobilities exceeds two orders of magnitude.[9] Herein, we apply the model to understand the effect of postproduction heat treatment at different temperatures on the performance of composite P3HT:PCBM solar cells, and quantify the parameters that limit the device performance. To anticipate the results, the most important factor that leads to an increase in J_{SC} of up to a factor of five is the enhancement of the hole mobility of P3HT in the blend by more than three orders of magnitude. For partially annealed devices (annealed at temperatures lower than the optimum), the difference in electron and hole mobility is too large, and we demonstrate that J_{ph} is strongly limited by the buildup of space-charge. This regime can be discriminated by the 1/2 power dependence of the J_{ph} on voltage (as inferred in Fig. 1 by the curve at 70 °C) and the 3/4 power dependence on light intensity.[9] In the space-charge limit, the FF is not able to exceed 0.42, being approximately constant when varying light intensity and temperature. At optimum annealing temperature (above 110 °C), the difference in electron and hole mobilities is reduced to, typically, a factor of 20 and, consequently, the space-charge no longer limits the performance under normal operating conditions. Here, the J_{ph} scales linear with light intensity, and the FF reaches values of 0.7. Furthermore, numerical simulation indicates that at short-circuit the dissociation efficiency of e–h pairs at the D/A interface is close to 90 %, which explains the large quantum efficiencies measured in P3HT:PCBM blends. These results are valuable for the design of new materials and further improvement of the performance of organic photovoltaic devices.

2. Results and Discussion

2.1. Charge-Carrier Transport in Composite P3HT:PCBM Films

Prior to the investigation of the photocurrent of the P3HT:PCBM blends, knowledge about the hole and electron mobilities is indispensable. Recently, much work has been done to measure the hole mobility of pristine P3HT using field-effect transistors (FETs),[18,19] time-of-flight (TOF) photocurrent measurements,[20] and space-charge-limited (SCL) current in a sandwich structure as solar cells or light-emitting diode configurations.[21] The measured hole mobility ranges from 10^{-8} m^2 V^{-1} s^{-1} in TOF and SCL current, up to 10^{-5} m^2 V^{-1} s^{-1} in FETs. It should be noted that regioregular P3HT self-organizes into a crystalline structure and, owing to the π–π stacking direction, the charge (hole) transport is extremely efficient. Since in FET measurements the current travels in the plane of the film (parallel to the substrate), the anisotropy in the polymer-chain orientation contributes strongly to the difference in the mea-

ADVANCED FUNCTIONAL MATERIALS

sured mobility. Moreover, a different molecular weight of P3HT, the presence of PCBM, and/or the applcation of a thermal treatment will also affect the measured electron and hole mobilities.[19,21] Therefore, the relevant values for charge-carrier mobilities can only be obtained when measured in the same configuration and experimental conditions as used in an operational solar-cell device.

Previously, we have shown that electron and hole mobilities in the blend can be determined from current–voltage measurements by using electrodes that either suppress the injection of electrons or holes, resulting in hole- or electron-only devices, respectively.[8,22] In this section, we have applied this technique to measure either the hole or electron current in blends of P3HT:PCBM as a function of the annealing temperature of the spin-coated films. To fabricate the hole-only devices, palladium was evaporated as the top electrode in an indium tin oxide (ITO)/poly(3,4-ethylenedioxythiophene):poly(4-styrene sulfonate) (PEDOT:PSS)/P3HT:PCBM structure. The work function of PEDOT:PSS matches the highest occupied molecular orbital (HOMO) of P3HT at 4.9 eV, forming an Ohmic contact for hole injection,[11,21] whereas palladium strongly suppresses electron injection into PCBM owing to the large mismatch between its work function and lowest unoccupied molecular orbital (LUMO) of PCBM.[23] A schematic diagram of a hole-only device is shown in the inset of Figure 1a. In order to suppress the hole injection into P3HT, the bottom contact must have a low work function. Recently, we demonstrated that the work function of a noble metal (such as silver) can be modified using a self-assembled monolayer (SAM).[24] This technique works very well and successful electron-only devices were constructed using blends of MDMO-PPV:PCBM.[8] Therefore, similar electron-only devices were also constructed for the P3HT:PCBM blends, the schematic band diagram of such an electron-only device is presented as an inset in Figure 2b.

Figure 2 shows the experimental dark-current densities (J_D) of P3HT:PCBM blends that were measured in hole-only (Fig. 2a) and electron-only (Fig. 2b) devices for different annealing temperature performed on the completed device. For clarity, only the devices that were measured as cast, and after thermal annealing at 90 °C and 120 °C, are shown. The applied voltage was corrected for the built-in voltage (V_{BI}) and the voltage drop (V_{RS}) arising from the substrate's series resistance.[25] When the applied voltage is greater that V_{BI}, J_D throughout all devices scales quadratically with voltage, indicative of SCL transport. This observation is common for low-mobility, disordered semiconductors and it allows for a direct determination of the mobility.[8,21,22] For the electron- and hole-only devices the SCL current is approximated by[26]

$$J_{e(h)} = \frac{9}{8}\varepsilon_0\varepsilon_r\mu_{e(h)}\exp\left(0.891\gamma_{e(h)}\sqrt{\frac{V}{L}}\right)\frac{V^2}{L^3} \quad (1)$$

where $J_{e(h)}$ is the electron (hole) current, $\mu_{e(h)}$ the zero-field mobility of the electrons (holes), $\gamma_{e(h)}$ the field activation factor, ε_0 the permittivity of free space, ε_r the relative permittivity of the material, and L the thickness of the active layer. The experimental data in Figure 2 were fitted using Equation 1, and the results are shown by the solid lines.

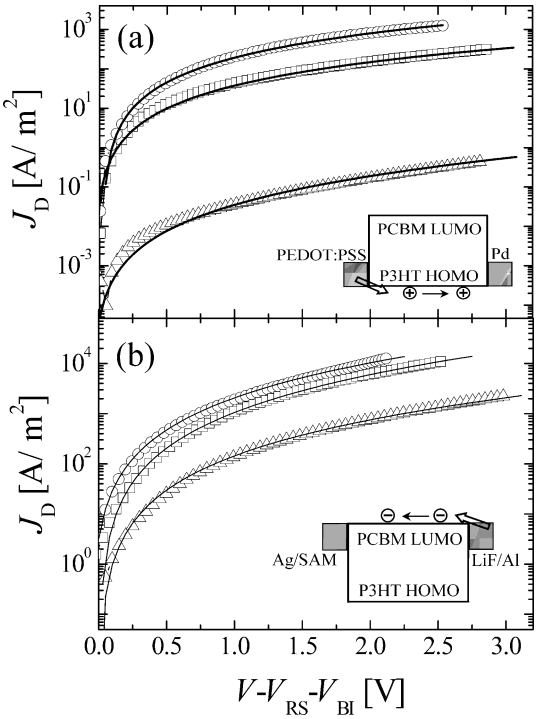

Figure 2. Experimental dark-current densities (J_Ds) of the 50:50 wt.-% P3HT:PCBM-blend devices measured at room temperature in the hole-only (a) and electron-only (b) device configuration, as shown by the inset schematic diagrams. The symbols correspond to different annealing temperatures of the photoactive layer as follow: as-cast (△), 90 °C (□), and 120 °C (○), respectively. Here, the thickness of the annealed hole-only devices (□,○) is 120 nm, whereas for the other devices is 220 nm. The solid lines represent the fit using a model of single-carrier SCL current with field-dependent mobility (Eq. 1). The J_D–V characteristics are corrected for the voltage drop over the contacts (V_{RS}) and the built-in voltage (V_{BI}) that arises from the work-function difference between the contacts.

Figure 3 shows the calculated zero-field mobility of electrons and holes in 50:50 wt.-% blends of P3HT:PCBM devices as a function of the annealing temperature. For comparison, the hole mobility of pristine P3HT, measured under the same experi-

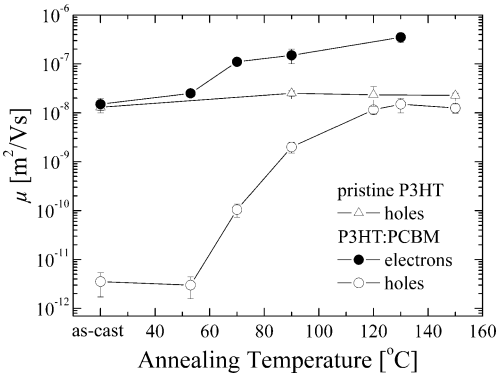

Figure 3. Room-temperature electron (●) and hole (○) zero-field mobilities in 50:50 wt.-% blends of P3HT:PCBM as a function of postproduction annealing temperature of the completed devices. For comparison, the hole mobility measured in pristine P3HT devices (△) is also shown. The mobilities were calculated from the SCL current measured using the electron- and hole-only device configuration (Fig. 2).

mental conditions, is also shown. It appears from Figure 3 that the hole mobility in pristine P3HT is hardly affected by thermal annealing, with a typical value of $(1.4–3.0)\times10^{-8}$ $m^2 V^{-1} s^{-1}$. This mobility was found to be completely field-independent ($\gamma_h = 0$) and fully consistent with previously reported values for high-molecular-weight P3HT (such as the one used here).[21] In contrast, the hole mobility of P3HT in the blend is strongly affected by the presence of PCBM and it drops almost four orders of magnitude for an as-cast device. Upon annealing, however, the mobility starts to increase sharply with an onset at 50–60 °C, followed by saturation to approximately the value of the pristine polymer when the devices are annealed above 120 °C. Also, the field activation factor gradually decreases from $\gamma_h \approx 4.0\times10^{-4}$ $(V m^{-1})^{-1/2}$ for the as-cast film to $\gamma_h = 0$ $(V m^{-1})^{-1/2}$ for the devices annealed above 90 °C. Moreover, the electron mobility of PCBM in the blend is also affected by thermal annealing: for as-cast films the electron mobility is $(1–2)\times10^{-8}$ $m^2 V^{-1} s^{-1}$, typically a factor of 5000 higher than the hole mobility. As a result, the charge transport in as-cast films is strongly unbalanced and the current is fully dominated by the electrons. Interestingly, for the same volume fraction the electron mobility in as-cast P3HT:PCBM films resembles the value measured previously in MDMO-PPV:PCBM blends.[8] However, thermal annealing of P3HT:PCBM films results in an electron mobility enhanced by, typically, a factor of 30, with an onset corresponding to the same temperature observed for the hole mobility, as inferred from Figure 3.

Furthermore, modulated differential scanning calorimetry (DSC) has been used to assess the degree of crystallinity of the particular batch of regioregular P3HT used in these experiments. The DSC thermogram, measured using a scan rate of 2 K min^{-1}, reveals two weak changes in the gradient at ≈50 °C, which correspond to the onset of the side-chain melting temperature (T_{sc}), and at ≈125 °C, corresponding to the onset of the glass-transition temperature (T_g); Furthermore, a strong melting peak appears at ≈215 °C. These results are valuable for understanding the film-formation mechanism and the charge transport in these blends. It has been shown that regioregular P3HT self-organizes into microcrystalline lamellae structure, forming well-defined whiskerlike entities.[27–29] This predominantly crystalline film may already have been formed in the pristine P3HT directly after the spin-coating process and thermal annealing does not further improve the crystallinity. As a consequence, the hole mobility in the pristine P3HT is not expected to change after the annealing of the film. However, in the blend devices, the presence of PCBM molecules might prevent immediate crystallization of P3HT after the spin-coating process, resulting in a more amorphous film. This hypothesis is strengthened by a recent preposition made by Yang et al. who argue that a rather homogeneous nanoscale distribution of PCBM in the P3HT matrix is present in the film as cast.[15] Consequently, the conformation of the P3HT chains and the way they pack together results in a weak interchain interaction which strongly suppresses the hole mobility. Upon thermal annealing, slow crystallization of P3HT takes place and demixing between P3HT and PCBM is observed,[15] which leads to an enhanced charge transport. As a result, interpenetrating networks composed of P3HT crystals and aggregated nanocrystalline PCBM-rich domains are formed, which provide continuous pathways in the entire photoactive layer for efficient electron and hole transport. It appears from Figure 3 that the onset in both electron and hole mobility in P3HT:PCBM blends corresponds with T_{sc}. Above this temperature the side-chain of P3HT melts, allowing PCBM molecules to diffuse and form nanocrystalline domains of pure PCBM which subsequently result in an enhanced electron transport, as seen experimentally. Moreover, heating above T_g allows the freely formed chains in the polymer melt to disentangle into a lower-energy conformation. This presumed straightening and crystallization of the polymer strands upon annealing will lead to a more planar π–π stacking, thereby increasing the interchain interaction and hole mobility. In section 2.3, the experimental charge-carrier mobilities of Figure 3 will be used to analyze the photocurrent generation and the performance of the solar cells as a function of annealing temperature.

2.2. Optical Absorption Spectra

Absorption spectra of pristine P3HT and P3HT:PCBM mixtures were investigated before and after thermal annealing, using a Perkin–Elmer Lambda 900 UV-vis/NIR spectrometer. All films were measured in transmission mode on glass/ITO/PEDOT:PSS substrates and subsequently corrected for substrate absorption. The absorption spectra of the blends (Fig. 4) clearly show two peaks: one at 335 nm corresponding to the PCBM, while the other peak (500–550 nm) represents the contribution of P3HT. The latter shows a pronounced red-shift upon thermal annealing, while the peak of PCBM remains unchanged. Similar results have been reported by other authors.[10,30] Furthermore, the mobility measurements presented in Figure 3, correlated with the morphology investigations[15,27–29] indicate that there is a change in the physical conformation of the P3HT chains. As a result, the packing

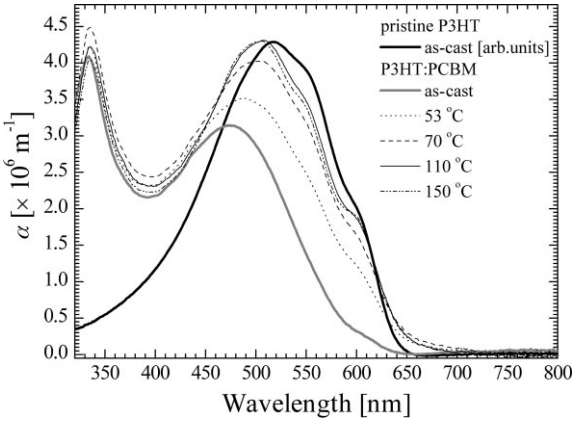

Figure 4. UV-vis absorption-coefficient (α) spectra of P3HT:PCBM blend films, as-cast, and for different annealing temperatures (see legend). The annealing time was 4 min. For a better comparison, the absorption of a pristine P3HT film as cast is also shown (in arbitrary units). All films were measured on a glass/ITO/PEDOT:PSS substrate and corrected for substrate absorption.

ADVANCED FUNCTIONAL MATERIALS

together of P3HT in the presence of PCBM is different, relative to that in pristine P3HT films, thereby altering the relevant optical and electronic properties that are critical for the operation of these devices. This change in the conformation is also reflected in the absorption spectra of the blend films. As shown in Figure 4, the UV-vis absorption-coefficient spectra of the blend film as cast is strongly blue-shifted with respect to the spectrum of pristine P3HT. This shift might originate from a tighter chain coil, produced by twisting of the polymer backbone or broken conjugation in the presence of PCBM, resulting in segments with a shorter conjugation length and weaker interchain interaction. This is consistent with absorption spectra of pristine P3HT, which show no change after annealing, but, rather, a small increase in the absorption intensity (not shown). Upon annealing, the PCBM demixes from the P3HT, as inferred by Yang et al.,[15] thereby increasing the degree of crystallinity of the polymer and consequently undergoes a noticeable shift to the red, approaching the spectrum of the pristine polymer. It appears from Figure 4 that the shift of the optical absorption is maximized when the devices are annealed above 100 °C, which closely corresponds with the temperature at which the hole mobility in the blend begins to approach that of the pristine polymer.

Nevertheless, the net effect of the red-shift of the optical absorption upon annealing, with respect to the nontreated film, is that it will improve the spectral overlap with solar emission, resulting in an increased absorption in the device. The absorption coefficients (α) shown in Figure 4 can be used to estimate the amount of additionally absorbed photons upon thermally annealing the P3HT:PCBM BHJ solar cell. The calculation was done using the following equation (as a function of wavelength, λ):

$$I_{\mathrm{abs}}(\lambda) = I_0(\lambda)[(1 - 10^{-\alpha(\lambda)L}) + R(\lambda) \cdot 10^{-2\alpha(\lambda)L}(10^{-\alpha(\lambda)L})] \quad (2)$$

where I_{abs} is the fraction of absorbed photons, I_0 the light-source spectrum, and R the reflectivity of the top-electrode material (Al; $R \approx 92$ % on the involved spectral range).[31] The results of the calculations are shown in Figure 5 together with the light-source spectrum used in our measurements (I_0), for a device with a thickness (L) of 96 nm. After integrating the area under the curves it appears that the annealed device improves light harvesting by approximately 60 % relative to the nontreated device. In the next section this information will be used to explain the enhanced photocurrent generation in the annealed devices.

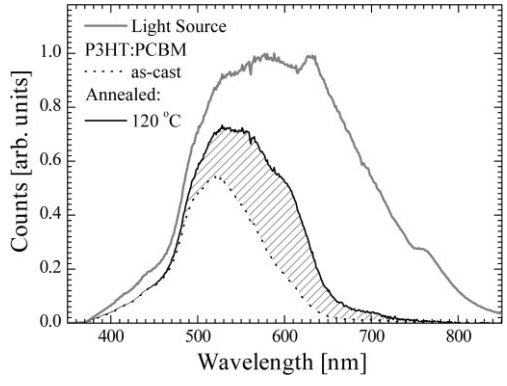

Figure 5. Fraction of absorbed photons (I_{abs}) from the excitation source (I_0) by a P3HT:PCBM solar cell with a thickness of $L = 96$ nm. The calculation is done for the film as cast and after annealing at 120 °C (see legend) using the absorption coefficients (α) given in Figure 4.

2.3. Device Characterization under Illumination

2.3.1. The Effect of Thermal Annealing on Solar-Cell Performance

After the investigation of the charge transport and optical absorption spectroscopy we proceeded with the analysis of the solar-cell performance upon thermal annealing of the photoactive P3HT:PCBM layer. The devices consisted of 50:50 wt.-% P3HT:PCBM blends which were spin-coated from a single chloroform solution on an ITO/PEDOT:PSS substrate, followed by the evaporation of a thin samarium (8 nm)/aluminum (100 nm) top electrode. The annealing was performed, after completing the devices, in a N_2 atmosphere on a hot plate for a duration of four minutes. The active layer thickness ranged from 94 to 97 nm for all fabricated devices.

Figure 6 shows the variation of the principal photovoltaic parameters (i.e., their mean values together with the standard deviations) as a function of annealing temperature. The devices were illuminated from a halogen lamp with the spectral range and shape shown in Figure 5, calibrated using a silicon diode at

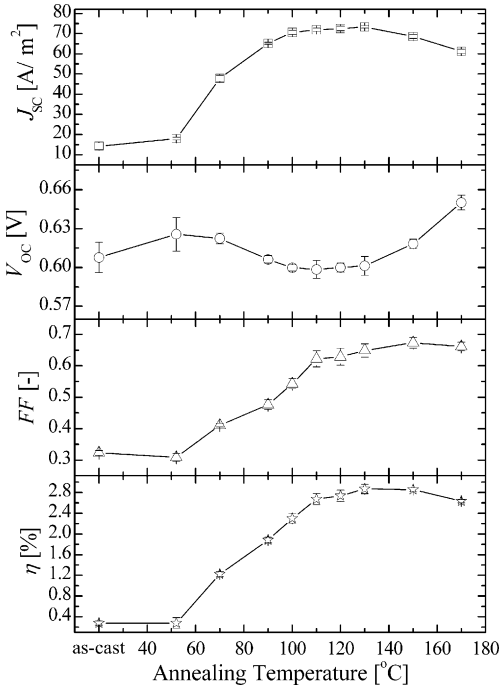

Figure 6. Device performance of the 50:50 wt.-% P3HT:PCBM blends, under illumination from a halogen lamp, as a function of annealing temperature. The annealing was done on a hot plate in a N_2 atmosphere for 4 min. The thickness of all devices (L) ranged from 94 to 97 nm.

an intensity of approximately 1.15 Sun (115 mW cm^{-2}). The open-circuit voltage (V_{OC}) is relatively constant and varies less than 40 mV, showing a slight increase above 150 °C. Conversely, all remaining device parameters show a very fast increase with annealing temperature between 50 and 110 °C, followed by saturation. The onset of this enhancement strongly corresponds with the onset in the hole mobility of P3HT in the blend (Fig. 3), and occurs above T_{sc}. Furthermore, the saturation appearing in J_{SC}, FF, and η when annealed above 110 °C seems also to be related to the P3HT hole mobility. Above this annealing temperature the enhancement of the hole mobility of P3HT in the blend is maximized, and, consequently, the difference between the electron and hole mobilities is reduced, typically, to a factor of 20, leading to a much more balanced transport. In particular, the thermal treatment produced a fivefold enhancement of J_{SC}, a twofold increase of FF, and, consequently, a tenfold gain of η (as inferred from Fig. 6). It is worth mentioning that the η does not show a clear optimum at a particular annealing temperature, but is, rather, unchanged above 110 °C, in contrast with previously reported results.[10–12,15] We have identified that the source of the decreasing performance in these studies, when annealing above 130 °C, is the degradation of the LiF/Al top electrode. With a samarium cathode, as used in our study, this problem does not occur. As a further test we applied a LiF/Al cathode after the thermal-annealing step, and in that case also no decrease in performance was observed at higher annealing temperatures.

To identify the main origin of the performance enhancement as a function of annealing treatment, the effects of enhanced absorption owing to the absorption red-shift and the increased charge transport must be disentangled. With regard to the absorption, the shaded area in Figure 5 represents the additional fraction of photons absorbed by the film upon annealing. This shaded area is now plotted in Figure 7 in the form of the relative enhancement with respect to the untreated film for all annealing temperatures. Thus, Figure 7 shows that, compared to the untreated film, the total absorption increases by a factor of 1.6 for films annealed above 100 °C. In a recent study we showed that at high reverse voltages the photocurrent is fully saturated, being independent of voltage and temperature.[8,17] In this regime the saturated photocurrent is given by $J_{sat} = q\, G_{max}\, L$, with q the electric charge and G_{max} the maximum generation rate of e–h pairs by the solar-cell device. In this saturated regime all bound e–h pairs are separated into free carriers and consequently G_{max} is only governed by the amount of absorbed photons. In Figure 7, the relative increase of G_{max}, determined from the saturated photocurrent at high effective voltages ($(V_0 - V) > 10$ V) as shown in Figure 1, is plotted. G_{max} ranges from 3.56×10^{27} m^{-3} s^{-1} for as-cast devices to 5.7×10^{27} m^{-3} s^{-1} for the annealed (120 °C) devices. Figure 7 convincingly demonstrates that the increase in G_{max} is completely a result of the enhanced absorption, which implies that all additionally generated excitons in the P3HT phase of the blend are able to dissociate at the D/A interface and form e–h pairs. This is further supported by a recent preposition made by Yang et al. who showed that the fibrillar-like P3HT crystals that form upon annealing at 120 °C do not significantly reduce the interface area with the electron acceptor PCBM.[15] The origin of the decrease of G_{max} above 130 °C is presently not known. Thus, as a first step, we have demonstrated that the increase of the photocurrent with a factor of 1.6 at high reverse voltages is solely the result of an increase of the optical absorption. However, for comparison, J_{SC} increases by a factor of five upon annealing, as shown in Figure 6. Therefore, this strong increase, together with the enhancement of the FF, cannot be attributed to the absorption increase of the film upon annealing. An important question that remains is what mechanism dominates such a strong enhancement in J_{SC} and FF of the cell and what limits the performance of an as-cast device or a device annealed at lower temperature.

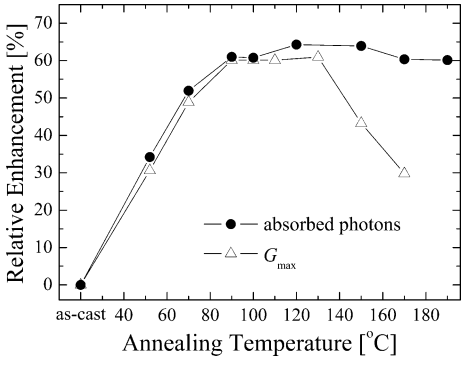

Figure 7. Relative enhancement [%] of the absorbed photons and maximum generation rate (G_{max}) for an annealed compared to an as-cast device, as a function of annealing temperature. The absorption was calculated from the shaded area in Figure 5, whereas G_{max} was determined from the saturation of the photocurrent ($J_{sat} = q\, G_{max}\, L$) at high effective voltages ($V_0 - V$) shown in Figure 1.

Recently, we have demonstrated that the photocurrent in polymer/fullerene blends can be limited by the buildup of space-charge, even under normal operation conditions (1 Sun illumination). This SCL photocurrent occurs when the difference between electron and hole mobility is too large.[9] The fingerprints of a SCL photocurrent are its square-root dependence on voltage and a 3/4 dependence on light intensity.[9] The mobility measurements presented in Figure 3 show that there is a greater than two orders of magnitude difference between the electron and hole mobilities in as-cast devices and devices annealed up to 90 °C. As expected, the photocurrents shown in Figure 1 indeed exhibit a square-root dependence on voltage for both the as-cast film and the device annealed at 70 °C. In the following section, the dependence of the photocurrent on light intensity of devices annealed at low temperatures is further investigated.

2.3.2. Light-Intensity Dependence

To gain further insight in the operation of P3HT:PCBM devices and quantify the limiting parameters, the light-intensity (P_{light}) dependence of the photocurrent has been studied for the device annealed at 70 °C). The P_{light} was varied from 1000 W m^{-2} (upper curve) down to 76 W m^{-2} using a set of neutral density filters with a constant optical density over the

ADVANCED FUNCTIONAL MATERIALS

spectral range of the light source (shown in Fig. 5). Subsequently, the resulting spectrum of each filter-lamp combination was recorded and integrated over the absorption spectrum of the blend P3HT:PCBM film, which gave the intensity. Therefore, the generation rate (G) of e–h pairs is proportional to the light intensity ($G \propto P_{light}$). Qualitatively, J_{ph} follows the power-law dependence:

$$J_{ph} \propto P_{light}^{S} \tag{3}$$

where the exponent S ranges from 0.75 in the case of SCL photocurrent to 1.0 for the space-charge-free limit.[9]

Figure 8 shows the J_{ph}–$(V_0 - V)$ characteristics of the P3HT:PCBM device, after thermal annealing at 70 °C as shown in Figure 1, as a function of P_{light}. It is observed that for $(V_0 - V) < 0.03$ V, the J_{ph} shows linear dependence on voltage at all light intensities, which is caused by the opposite effects of drift and diffusion of charge carriers.[9,16,17] Above 0.03 V, however, a square-root dependence on voltage of the experimental J_{ph} is observed, as is predicted for blends with a large difference in electron and hole mobilities.[9] At even larger voltages the J_{ph} shows a clear transition to the saturation regime where it becomes limited by the field (E) and temperature (T) dependence of the dissociation of bound e–h pairs; $J_{ph} = q\,G(E,T)\,L$.[17] These results are distinctly different when the devices are annealed at higher temperature, where the electron and hole transport is more balanced. In that case, no square-root dependence of J_{ph} is observed, as seen in Figure 1 in the curve at 120 °C. Moreover, it appears from Figure 8 that J_{ph} shows weaker P_{light} dependence in the square-root regime compared to the saturation regime. Figure 9 displays, on a double-logarithmic scale, the experimental J_{ph} taken from Figure 8 as a function of light intensity for two different voltages; at $(V_0 - V) = 0.1$ V in the square-root regime and at $(V_0 - V) = 3$ V in the saturation regime. The slope S determined from the linear fit (lines) to the experimental data (as shown in Fig. 9) clearly proves that J_{ph} is limited by the buildup of space-charge in the square-root regime and becomes space-charge-free in the saturation regime.[9] Because the J_{SC} (indicated by the arrow in Fig. 8) at high light intensity falls in the square-root part of the J_{ph}–$(V_0 - V)$ characteristics, the device is fully limited by the buildup of space-charge between the open- and short-circuit points. In this case the FF of the device is reduced to less than 0.42 and the J_{SC} approaches a 3/4 P_{light} dependence ($S \approx 0.75$). By decreasing the light intensity, the transition voltage from square-root to saturation moves to lower values and the device is only partially limited by the space-charge.[9] As a consequence, the FF of the device increases and the J_{SC} approaches a linear dependence on light intensity ($S \approx 1$).

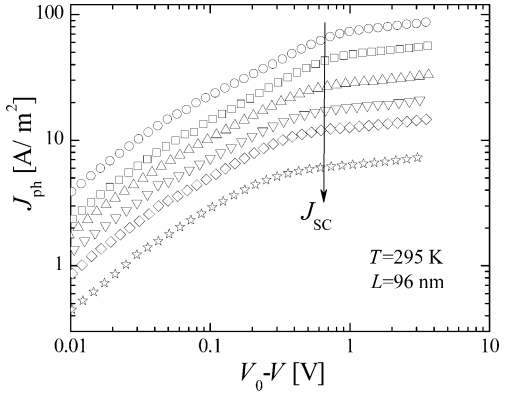

Figure 8. Light-intensity dependence of the photocurrent (J_{ph}) versus effective applied voltage ($V_0 - V$) of the device thermally annealed at 70 °C. The intensity was varied from 1000 (upper curve) down to 76 W m^{-2}, whereas the arrow indicats the position of the short-circuit current (J_{SC}).

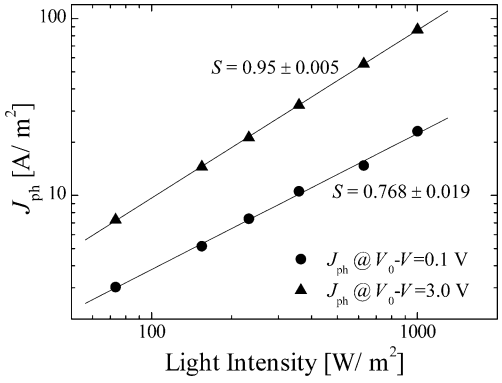

Figure 9. Light-intensity dependence of the photocurrent (J_{ph}) taken from Figure 8 at an effective voltage of $(V_0 - V) = 0.1$ V and $(V_0 - V) = 3.0$ V (symbols). The slope (S) determined from the linear fit (solid lines) to the experimental data is written on the figure.

From Figure 8 it is clear that the buildup of space-charge dramatically reduces the device performance, since it causes a fundamental limitation on FF and J_{SC}. This space-charge is a direct result of the unbalanced transport of electrons and holes in the device. Owing to the strongly increased hole mobility, leading to a better balanced transport, this limitation is prevented under normal operating conditions in the device annealed above 110 °C. The absence of space-charge effects is further evidenced by a completely linear ($S = 1.0$) dependence of J_{ph} on P_{light} (data not shown). Thus, the enhancement in the device efficiency by a factor of ten upon thermal annealing is mainly a result of the improved hole mobility of P3HT inside the blend by more than three orders of magnitude, rather than by improving light harvesting (with ≈60 %). With increased hole transport, the devices recover from the space-charge limitation to become space-charge-free, as a result of a more balanced transport. As shown in Figure 1, the absence of the square-root voltage dependence in the device annealed at 110 °C leads to a strong enhancement of both FF and J_{SC}. In order to fully quantify the device performance we have analyzed the photocurrent generation in P3HT:PCBM solar cells further, with the help of numerical simulations.[16]

2.3.3. Numerical-Simulation Results

Recently, we have shown that the photocurrent in conjugated polymer/fullerene blends is dominated by the dissociation probability [$P(E,T)$] of e–h pairs at D/A interface, which is a field- and temperature-dependent process.[17] In the saturation

regime the photocurrent is given by $J_{ph} = q\,G(E,T)\,L$, where $G(E,T) = P(E,T)\,G_{max}$. The probability P depends on the initial e–h separation distance (a) and the decay rate of bound pair (k_F). Once separated, the free electron and hole can again bimolecularly recombine at the interface to form a bound pair with a rate constant (k_R),[32] which may dissociate again during its lifetime. To fit the experimental data, the $G(E,T)$ has been taken into account in a numerical model which solves the steady-state continuity equations for electrons and holes including diffusion, recombination, and space-charge effects via the Poisson equation.[16] For MDMO-PPV:PCBM-blend devices, this model quantitatively explained the behavior of the photocurrent as a function of temperature and PCBM composition.[8,16,17] The most limiting factor in these blends is the dissociation efficiency of bound e–h pairs across the D/A interface, which is only 60 % at room temperature under short-circuit conditions. To calculate the photocurrent for the P3HT:PCBM devices, the input parameters required in the model are: the charge-carrier mobilities of electrons and holes, the spatially averaged dielectric constant (ε_r) of P3HT and PCBM, the initial (e–h) separation distance (a), the bound-pair lifetime (k_F^{-1}), the maximum generation rate (G_{max}), and the semiconductor bandgap (E_g). Since ε_r for P3HT and PCBM are know, the E_g is estimated from the HOMO(P3HT)–LUMO(PCBM) difference, G_{max} is determined from the saturation of the photocurrent (Fig. 7), and the charge-carrier mobilities are presented in Figure 3; the only adjustable parameters of the model that remain are a and k_F^{-1}. Similarly to MDMO-PPV:PCBM blends, a and k_F can be independently determined from the field-dependent dissociation probability $P(E,T)$ by fitting the temperature dependence of the photocurrent.[17] Under sufficient applied reverse bias (≤ –3 V), all e–h pairs are dissociated and the J_{ph} approaches full saturation, being field- and temperature-independent. This saturation allows determination of a. Subsequently, k_F is determined by fitting the field dependence of the J_{ph}.

Figure 10 shows the temperature dependence of the J_{ph} versus $V_0 - V$ of a P3HT:PCBM device after thermal annealing at 120 °C. It appears from the figure that the experimental J_{ph} shows an extremely weak field and temperature dependence in the saturation regime for $(V_0 - V) > 0.3$ V, where $J_{ph} = q\,P(E,T)\,G_{max}\,L$. For effective voltages $(V_0 - V) > 3$ V, the experimental J_{ph} clearly approaches full saturation meaning that all e–h pairs are dissociated ($P \rightarrow 1$) and $J_{sat} = qG_{max}\,L$. By comparing the J_{ph} with the experimentally observed J_{sat}, the dissociation probability at any effective voltage can be read directly from the experimental data. For example, under short-circuit conditions ($V = 0$ V), the dissociation probability of e–h pairs (P_{SC}) is close to 0.9 (at room temperature), which is considerably larger than the previously reported value for MDMO-PPV:PCBM devices ($P_{SC} = 0.6$).[17] The solid lines in Figure 10 represent the numerical calculation of J_{ph} including the field- and temperature-dependent generation rate G(E,T). From the best fit to the experimental data an e–h separation distance of $a = 1.8$ nm and room-temperature bound-pair decay lifetime of $k_F^{-1} \approx 50$ µs were obtained. Compared to the MDMO-PPV:PCBM system it is observed that both a and k_F^{-1} are larger,[8,17] leading to an enhanced dissociation probability. Because of this efficient dissociation, the field dependence of J_{ph} is extremely weak, and if we think in terms of photocurrent–voltage characteristics, it is now possible to obtain a FF as high as 0.7, as observed experimentally (Fig. 6). The microscopic origin of the enhanced dissociation is the subject of further study.

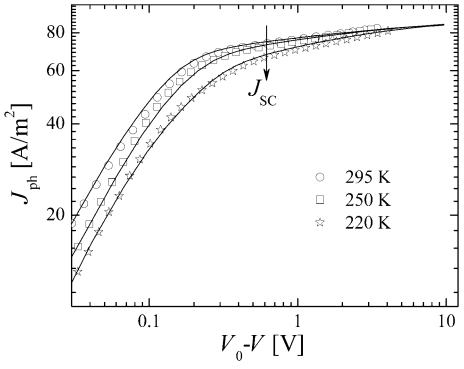

Figure 10. Temperature dependence of the photocurrent (symbols) versus effective applied voltage ($V_0 - V$) for a 50:50 wt.-% P3HT:PCBM device with a thickness of 120 nm, annealed at 120 °C for 4 min. The solid lines represent the numerical calculation using the model form Koster et al. [16].

Next, we have used the numerical model to calculate the J_{ph} of the P3HT:PCBM devices as a function of annealing temperature. The only input parameters that change with annealing temperature are the mobilities (Fig. 3) and the G_{max} (Fig. 7), as obtained from the fully saturated part of the J_{ph}. Figure 11a shows the experimental J_L–V characteristics under illumination of the devices presented in Figure 6 as a function of thermal-annealing treatment (symbols). For clarity, not all curves are shown. Assuming the same e–h separation distance (a) and lifetime (k_F^{-1}), the model exactly predicts the photocurrent at any annealing temperature, as seen by the solid lines in Figure 11a. From the excellent agreement between simulated and experimental J_{ph}, it follows that the model accurately predicts the FF and η of all these cells. Moreover, Figure 11b shows the calculated P_{SC} at all annealing temperatures. Weak dissociation of bound e–h pairs is observed for as-cast or devices annealed at low annealing temperature as a result of the low hole mobility of P3HT in the blend. The maximum dissociation efficiency of ≈88 % is reached when annealed above 110 °C, which corresponds to the maximum enhancement in hole transport. Furthermore, the good agreement of the numerical simulation with the experimental data presented above enables us to predict the behavior of the P3HT:PCBM devices under any other conditions. For example, with the measured electron and hole mobilities of the device annealed at 120 °C, the numerical calculations indicate that space-charge will fully limit the J_{ph} only at intensities over 30 Sun illumination in 100 nm film.

Finally, these results allow a true comparison between P3HT:PCBM (1:1)- and MDMO-PPV:PCBM (1:4)-blend devices. With respect to the charge transport, the P3HT-based devices (Fig. 3) have similar mobilities to those measured recently in MDMO-PPV:PCBM devices.[8,22] However, a larger

ADVANCED FUNCTIONAL MATERIALS

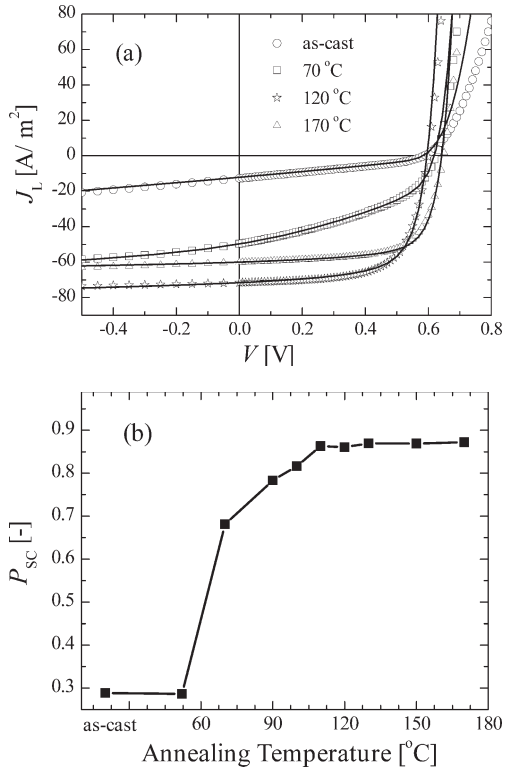

Figure 11. a) Room-temperature J_L–V characteristics under illumination of the P3HT:PCBM devices at different annealing temperatures (symbols). The solid lines represent the numerical calculation. b) Dissociation probability (P_{SC}) under short-circuit conditions at all annealing temperatures.

volume fraction of absorbing material (P3HT) combined with more red-shifted absorption increases the maximum rate of charge-carrier generation (G_{max}) in 50:50 wt.-% P3HT:PCBM devices by more than a factor of two, as compared to the 20:80 wt.-% MDMO-PPV:PCBM devices.[8] Combining this with a higher separation efficiency of photogenerated bound e–h pairs under short-circuit conditions increases the J_{SC} by more than a factor two for the P3HT-based devices. Also, the FF of the P3HT:PCBM solar cells is larger with respect to the values measured in MDMO:PCBM devices, as a result of a weaker field dependence of the photocurrent. The most limiting factor of all P3HT-based devices remains, however, the V_{OC}, which is approximately 40 % lower as compared to that of the MDMO-based devices. However, the increase in current and FF make up for the loss in V_{OC} and, therefore, the power efficiencies of P3HT:PCBM cells are significantly higher.

3. Conclusions

We have analyzed the charge transport and photogeneration in regioregular poly(3-hexylthiophene):methanofullerene (P3HT:PCBM) solar cells. A tenfold increase in power conversion efficiency was obtained by simply annealing the devices at a temperature above 110 °C for 4 min. The most important factor in obtaining these efficiencies was found to be the enhancement in hole mobility in the P3HT phase of the blend by more than three orders of magnitude, relative to the untreated device. For the as-cast devices, or devices annealed at a temperature lower than optimum (< 110 °C), the difference in electron and hole transport in the blend is too large and the photocurrent is strongly limited by the buildup of space-charge. Consequently, the devices are hindered by the fundamental electrostatic limit and the fill factor of the cells can not exceed ≈42 %. At optimum annealing temperature (above 110 °C), the difference in electron and hole mobility is reduced to typically a factor of 20 and, consequently, the space-charge no longer limits the performance under normal operation conditions leading to fill factors as high as ≈70 %. Furthermore, numerical simulations indicate that at short-circuit the dissociation efficiency of bound electron–hole pairs at the donor/acceptor interface is close to 90 %, which explains the large quantum efficiencies measured in P3HT:PCBM blends. These results are valuable for the design of new materials and further improve the performance of organic photovoltaic devices.

4. Experimental

4.1. Materials and Solutions

The regioregular poly(3-hexylthiophene) (P3HT, electronic grade; regioregularity greater than 98.5 %; received from Rieke Metals Inc.) was dissolved in distilled toluene, dedoped with hydrazine at 60 °C, and precipitated in methanol. The fraction collected was Soxhlet extracted for at least 64 h with methanol, *n*-hexane, CH_2Cl_2, and finally with $CHCl_3$. The chloroform fraction was precipitated in methanol, dried under vacuum and stored in the glove box under a N_2 atmosphere. The typical weight-average molecular weight is $M_w \approx 50\,000$ g mol^{-1}. The thermal transition behavior of P3HT powders was measured using modulated differential scanning calorimetry (DSC) with a scan rate of 2 K min^{-1}. The [6,6]-phenyl C_{61}-butyric acid methyl ester (PCBM) synthesized by the University of Groningen (The Netherlands) was used as received. To study the device performance, blend solutions of 50:50 wt.-% P3HT:PCBM were prepared using chloroform as the solvent at a solid contents varying from 8 to 12 mg mL^{-1}. The solutions were prepared in a N_2 atmosphere and rigorously stirred for more than 14 h on a hot plate at 50 °C.

4.2. Device Fabrication

All solar-cell devices used to investigate the photocurrent in this study were prepared using glass substrates coated with indium tin oxide (ITO; ≈ 15 Ω/square). To supplement this bottom electrode, a hole-transport layer of PEDOT:PSS (Baytron P VP Al 4083 grade) was spin-coated from an aqueous dispersion under ambient conditions, before the substrates were dried at 140 °C for 10 min. Next, composite layers of 50:50 wt.-% P3HT:PCBM were spin-coated on top of the PEDOT:PSS layer. To complete the solar-cell devices, 8 nm samarium (Sm) topped with aluminum (Al, 100 nm) electrodes were deposited by thermal evaporation under vacuum (1×10^{-7} mbar; 1 mbar = 100 Pa). The hole-only devices, used to investigate hole transport in P3HT:PCBM blends, were fabricated following the same procedure presented above except for the top electrode which was replaced with palladium (Pd; 40–50 nm). Electron-only devices were fabricated by spin-coating the active layer either on top of glass/Ag(50 nm)/self-

assembled monolayer (SAM) substrates, followed by the evaporation of a lithium fluoride (LiF; 1 nm)/Al(100 nm) top electrode. The preparation of the SAM is described elsewhere [24].

4.3. Measurements

The current-density versus voltage curves were measured in a N_2 atmosphere (< 1 ppm O_2 and < 1 ppm H_2O) with a computer-controlled Keithley 2400 Source Meter. To measure the current density under illumination (J_L), the devices were illuminated at the transparent ITO electrode by a white-light halogen lamp calibrated to approximately 1.15 Sun (115 mW cm^{-2}), with a Si diode. The thermal annealing of the devices was performed in the N_2 atmosphere on a hot plate for 4 min. The device temperature during the annealing process was measured using a point-contact thermocouple on top of a glass substrate, in order to exactly reproduce the sample conditions. The standard deviation in the annealing temperature was less than 2 °C. The optical absorption of the blend films and pristine P3HT was measured in transmission mode using a Perkin–Elmer Lambda 900 UV/Vis/NIR spectrometer. All films were measured on glass/ITO/poly(3,4-ethylenedioxythiophene): poly(styrene sulfonate) (PEDOT:PSS) substrates and subsequently corrected for substrate absorption.

Received: July 5, 2005
Final version: September 15, 2005
Published online: February 16, 2006

[1] J. Nelson, *Curr. Opin. Solid State Mater. Sci.* **2002**, *6*, 87.
[2] K. M. Coakley, M. D. McGehee, *Chem. Mater.* **2004**, *16*, 4533.
[3] H. Spanggaard, F. C. Krebs, *Sol. Energy Mater. Sol. Cells* **2004**, *83*, 125.
[4] C. J. Brabec, G. Zerza, G. Cerullo, S. De Silvestri, S. Luzzati, J. C. Hummelen, S. Sariciftci, *Chem. Phys. Lett.* **2001**, *340*, 232.
[5] J. M. Kroon, M. M. Wienk, W. J. H. Verhees, J. C. Hummelen, *Thin Solid Films* **2002**, *403*, 223.
[6] S. E. Shaheen, C. J. Brabec, N. S. Sariciftci, F. Padinger, T. Fromherz, J. C. Hummelen, *Appl. Phys. Lett.* **2001**, *78*, 841.
[7] M. M. Wienk, J. M. Kroon, W. J. H. Verhees, J. Knol, J. C. Hummelen, P. A. van Hal, R. A. J. Janssen, *Angew. Chem. Int. Ed.* **2003**, *42*, 3371.
[8] V. D. Mihailetchi, L. J. A. Koster, P. W. M. Blom, C. Melzer, B. de Boer, J. K. J. van Duren, R. A. J. Janssen, *Adv. Funct. Mater.* **2005**, *15*, 795.
[9] V. D. Mihailetchi, J. Wildeman, P. W. M. Blom, *Phys. Rev. Lett.* **2005**, *94*, 126 602.
[10] D. Chirvase, J. Parisi, J. C. Hummelen, V. Dyakonov, *Nanotechnology* **2004**, *15*, 1317.
[11] Y. Kim, S. A. Choulis, J. Nelson, D. D. C. Bradley, S. Cook, J. R. Durrant, *Appl. Phys. Lett.* **2005**, *86*, 063 502.
[12] F. Padinger, R. S. Rittberger, N. S. Sariciftci, *Adv. Funct. Mater.* **2003**, *13*, 85.
[13] C. J. Brabec, *Sol. Energy Mater. Sol. Cells* **2004**, *83*, 273.
[14] The photocurrent (J_{ph}; $J_{ph} = J_L - J_D$) is the measured current under illumination (J_L) corrected for the dark current (J_D), whereas V_0 is the compensation voltage. V_0 is defined as the voltage at which J_{ph} is zero: $V_{OC} < V_0 \leq V_{OC} + 0.048$ V for all the experiments presented throughout this paper.
[15] X. Yang, J. Loos, S. C. Veenstra, W. J. H. Verhees, M. M. Wienk, J. M. Kroon, M. A. J. Michels, R. A. J. Janssen, *Nano Lett.* **2005**, *5*, 579.
[16] L. J. A. Koster, E. C. P. Smits, V. D. Mihailetchi, P. W. M. Blom, *Phys. Rev. B* **2005**, *72*, 085 205.
[17] V. D. Mihailetchi, L. J. Koster, J. C. Hummelen, P. W. Blom, *Phys. Rev. Lett.* **2004**, *93*, 216 601.
[18] H. Sirringhaus, P. J. Brown, R. H. Friend, M. M. Nielsen, K. Bechgaard, B. M. W. Langeveld-Voss, A. J. H. Spiering, R. A. J. Janssen, E. W. Meijer, P. Herwig, D. M. de Leeuw, *Nature* **1999**, *401*, 685.
[19] R. J. Kline, M. D. McGehee, E. N. Kadnikova, J. S. Liu, J. M. J. Frechet, *Adv. Mater.* **2003**, *15*, 1519.
[20] Y. Kim, S. Cook, S. A. Choulis, J. Nelson, J. R. Durrant, D. D. C. Bradley, *Chem. Mater.* **2004**, *16*, 4812.
[21] C. Goh, R. J. Kline, M. D. McGehee, E N. Kadnikova, J. M. J. Fréchet, *Appl. Phys. Lett.* **2005**, *86*, 122 110.
[22] C. Melzer, E. J. Koop, V. D. Mihailetchi, P. W. M. Blom, *Adv. Funct. Mater.* **2004**, *14*, 865.
[23] V. D. Mihailetchi, P. W. M. Blom, J. C. Hummelen, M. T. Rispens, *J. Appl. Phys.* **2003**, *94*, 6849.
[24] B. de Boer, A. Hadipour, M. M. Mandoc, T. van Woudenbergh, P. W. M. Blom, *Adv. Mater.* **2005**, *17*, 621.
[25] For hole-only devices V_{BI} ($V_{BI} \approx 0.2$ V) was estimated from the difference between the work function of Pd and HOMO level of P3HT, whereas for electron-only devices $V_{BI} \approx 0$ V, since both Sm and LiF/Al form Ohmic contact with LUMO level of PCBM. The series resistance was determined from the reference devices fabricated without the photoactive layer and was found to be 4–5 Ω for electron-only devices, and 25–35 Ω for hole-only devices.
[26] P. N. Murgatroyd, *J. Phys. D* **1970**, *3*, 151.
[27] K. J. Ihn, J. Moulton, P. Smith, *J. Polym. Sci., Part B: Polym. Phys.* **1993**, *31*, 735.
[28] S. Malik, A. K. Nandi, *J. Polym. Sci., Part B: Polym. Phys.* **2002**, *40*, 2073.
[29] E. Mena-Osteritz, A. Meyer, B. M. W. Langeveld-Voss, R. A. J. Janssen, E. W. Meijer, P. Bauerle, *Angew. Chem. Int. Ed.* **2000**, *39*, 2680.
[30] N. Camaioni, G. Ridolfi, G. Casalbore-Miceli, G. Possamai, M. Maggini, *Adv. Mater.* **2002**, *14*, 1735.
[31] G. Hass, J. E. Waylonis, *J. Opt. Soc. Am.* **1961**, *51*, 719.
[32] L. J. A. Koster, V. D. Mihailetchi, P. W. M. Blom, unpublished.